Journal of Molecular Structure 1357 (2026) 145191

Contents lists available at ScienceDirect

Journal of Molecular Structure

journal homepage: www.elsevier.com/locate/molstr

Structural, supramolecular analysis, and photoluminescence properties of a new hydroxybenzohydrazide Schiff base

David Oliveros Garavito [a], Andrea Pastrana-Dávila [b], Javier Ellena [c], Pedro H.O. Santiago [c], Oscar Rojas [d], Dominik Pentlehner [d], Luis A. Illicachi [a,*], Richard D'Vries [e,*]

[a] Grupo de Investigación en Química y Biotecnología, Facultad de Ciencias Básicas, Universidad Santiago de Cali, Calle 5 # 62-00, Cali, Colombia
[b] Escuela de Ciencias Agrícolas, Pecuarias y del Medio Ambiente, Universidad Nacional Abierta y a Distancia (UNAD), Cra. 3 #2-55, Popayán, Cauca, Colombia
[c] São Carlos Institute of Physics, University of São Paulo, CEP 13.566-590, São Carlos, SP, Brazil
[d] Faculty of Chemical Technology and Business, Campus Burghausen Technical University of Applied Sciences Rosenheim Robert-Koch-Straße 28, Burghausen 84489, Germany
[e] Grupo de Investigación en Química de Productos Naturales, Departamento de Química, Facultad de Ciencias Naturales, Exactas y de la Educación, Universidad del Cauca, Calle 5 # 4–70, Popayán, Colombia

ARTICLE INFO

Keywords:
Hydroxybenzohydrazide
Schiff base
Supramolecular analysis
Crystalline material
Optical properties
Organic materials

ABSTRACT

This work presents the synthesis, spectroscopic characterization, and structural analysis of *N*′-((1*Z*,2*E*)-1,3-diphenylallylidene)-2-hydroxybenzohydrazide (**DAHH**). Comprehensive spectroscopic characterization was performed using ^{1}H and ^{13}C NMR, MS, FT-IR, and optical spectroscopy. Single crystal X-ray diffraction analysis shows that the new benzohydrazide derivative crystallizes in the monoclinic space group $P2_1/c$ with one molecule per asymmetric unit and general formula $C_{22}H_{18}N_2O_2$. The structural data enabled supramolecular analysis, showing that crystalline packing is formed by N-H···O and O-H···O hydrogen interactions. It also features weak T-shape C-H···π (edge-to-face) and C=C···π interactions. These results were corroborated and quantified using Hirshfeld surface and fingerprint plot analysis. The most abundant interaction is H···H dispersion (50.2%), followed by C···H (28%) and O···H (10.1%). Lattice energies and energy frameworks for the **DAHH** compound were also calculated. Finally, the luminescence properties of **DAHH** were studied.

1. Introduction

Benzohydrazide derivatives are an interesting organic platform with many applications in medicinal chemistry [1–4], material chemistry [5,6], and coordination chemistry [7–9]. They have a characteristic N-acyl hydrazone group (R1–CONHN=C-R2R3) that can present various functional groups at both the acetyl site (R1) and the hydrazone end (R2 and R3). Structurally, these compounds contain donor atoms, allowing the formation of coordination compounds. They also have a double bond, which is susceptible to isomerism [10,11]. Their applications are strongly related to the structure and the nature of the R1, R2, and R3 groups in the molecule. The presence of aromatic or heteroaromatic rings is associated with antibacterial, antifungal, and anticancer applications [4,12,13], while the presence of halogen atoms is associated with herbicide and insecticide applications [14,15].

On the other hand, benzohydrazides show promising applications in material chemistry, due to the wide range of possible structures which may exhibit high conjugation, π systems, and rigidity necessary for use as photoluminescent materials. Also, structurally it is possible to obtain asymmetric structures with different substituents on the *N*-acyl hydrazone group leading to non-centrosymmetric structures that may lead to optoelectronic properties, including optical transparency in the visible range, nonlinear optical (NLO) behavior with a high first-order hyperpolarizability (β_0) for uses such as optical limiting, and fluorescence properties suitable for sensors and OLEDs materials [16,17]. For example, molecules such as *N*, *N*′-diisonicotinoyl-2-hydroxy-5-methylisophthalaldehyde hydrazone [18] and 2-tosylamino-benzylidene-(2-benzo[d]thiazole) [19] are used as the emitting layer in OLED devices. In addition, several applications of these molecular systems include selective sensors for metal or molecular detection using naphthalimide- or isoniazid-based *N*-Acylhydrazone derivatives [20–22], quinoline-based acyl hydrazone for solid-state emission materials [23], and hydrazone-based switches [10].

Since the study of *N*-acylhydrazones derivatives as molecular

* Corresponding authors.
E-mail addresses: luis.illicachi00@usc.edu.co (L.A. Illicachi), richard.dvries@unicauca.edu.co (R. D'Vries).

https://doi.org/10.1016/j.molstruc.2025.145191
Received 25 September 2025; Received in revised form 11 November 2025; Accepted 28 December 2025
Available online 29 December 2025

materials has been underdeveloped and few structural reports are observed in the Cambridge Crystallographic Data Center (CCDC) database, this study focuses on the design and synthesis of a new molecular model with the basic characteristics of photoluminescence materials (conjugation, presence of π systems, and asymmetry) and relates the structural features with the electronic behavior. In this sense, the synthesis of *trans*-chalcone and salicylic hydrazide by condensation reaction was performed to obtain the *N*'-((1*Z*,2*E*)-1,3-diphenylallylidene)-2-hydroxybenzohydrazide **(DAHH)** compound. The spectroscopic characterization was performed by FTIR, UV-Vis, NMR (^{1}H and ^{13}C), and photoemission optical spectroscopy. Thermal characterization was performed by DSC analysis. The crystal structure of **DAHH** was determined by single-crystal X-ray diffraction, and the crystal packing and supramolecular structure were analyzed using Hirshfeld surface analysis, fingerprint plots, lattice energies, and energy frameworks. Finally, to understand the electronic and luminescent behavior of the new molecule, a preliminary emission analysis was conducted.

2. Materials and methods

2.1. Materials

All reagents and solvents used for synthesis were purchased from commercial suppliers (*Trans*-Chalcone 97 % and 2-Hydroxybenzohydrazide 97 % from Sigma-Aldrich, Ethanol 99.9 % for analysis from Emsure, and Hydrochloric acid 37 % from Merck) and used as received without further purification.

2.2. Characterization

FTIR spectra was recorded using an ATR Thermo Nicolet iS10 spectrophotometer (NICOLET iS10, DTGS and MCT detectors, spectral resolution: 4 cm^{-1}, Thermo Fisher Scientific, USA) in the 400–4000 cm^{-1} range with 32 scans. ^{1}H NMR (400 MHz) and ^{13}C NMR (100 MHz) spectra were obtained on a Bruker UltraShield Avance II spectrometer at room temperature (298 K) using $CDCl_3$ as the solvent. The chemical shift values (δ) are reported in parts per million (ppm), and the coupling constants (*J*) are reported in Hz. Thermal analysis (DSC) was performed in a TA instrument (Discovery DSC 250) under the following conditions: 25–500 °C temperature range, nitrogen atmosphere (50 mL min^{-1} Flow), and 20 °C min^{-1} heating rate.

Synthesis of *N*'-((1*Z*,2*E*)-1,3-diphenylallylidene)-2-hydroxybenzohydrazide (DAHH).

2 mmol of *trans*-chalcone and 2 mmol of salicylic hydrazide were dissolved in ethanol (10 mL) with 2 drops of 37 % HCl. The reaction mixture was stirred under reflux for 12 h. After cooling, a white solid was obtained. The product was obtained as white solid with a melting point of 182 °C with a yield of 90 %. FTIR (ATR) υ = 3262 (N-H), υ = 3055 (O-H), 1638 (C=O), ^{1}H NMR (400 MHz, $CDCl_3$) δ (ppm): 9.20 (s, 1H), 7.71–7.62 (m, 3H), 7.47–7.28 (m, 10H), 6.98 (d, *J* = 8.1 Hz, 1H), 6.73–6.71 (m, 2H), 6.48 (d, *J* = 16.4 Hz, 1H). ^{13}C NMR (100 MHz, $CDCl_3$) δ (ppm): 162.0, 139.3, 136.0, 134.8, 130.5, 130.2, 129.2, 129.0, 128.4, 128.3, 127.3, 119.0, 113.4. EI MS (70 eV): *m/z* 342 (12 %), 221 (57 %), 145(44 %), 121(100 %).

2.3. Single crystal X-ray diffraction analysis

Single crystals suitable for X-ray analysis were obtained by slow evaporation from a dichloromethane solution. Diffraction data for **DAHH** were collected at 100.00(11) K on a Rigaku Synergy-S diffractometer equipped with a HyPix-6000HE detector system, using CuKα (1.54184 Å) photon jet microfocus source. Cell parameters were obtained on all reflections using CrysAlisPro software [24]. Data integration and scaling were performed using CrysAlisPro software [24]. The structure was solved using the SHELXT [25] program and refined with SHELXL [26], both within the Olex2 system [27]. Non-hydrogen atoms were clearly resolved in the Fourier map. They were refined by full-matrix least-squares on F2, with anisotropic thermal parameters. Hydrogen atoms were stereochemically positioned and refined using the riding model [28,29]. The thermal ellipsoid diagram was prepared with Diamond [30]. The Mercury program was used to prepare artwork [31]. CCDC 2488400 contains the supplementary crystallographic data for this paper. These data can be obtained free of charge via http://www.ccdc.cam.ac.uk/conts/retrieving.html (or from the Cambridge Crystallographic Data Centre, 12, Union Road, Cambridge CB2 1EZ, UK; fax: +44 1223 336033).

2.4. Optical spectroscopy

Photoluminescence (PL) measurement was performed in dichloromethane (DCM) solution using a Horiba-Fluorolog 3 spectrofluorometer with FluorEssence software. Emission and excitation spectra were recorded using a Czerny-Turner spectrograph equipped with a R928 PMT for detection and a double monochromator with a Xenon lamp for excitation, respectively. No optical filters were used. The absorption spectrum was recorded using a Thermo Scientific Evolution 300 spectrophotometer. All optical spectra were recorded of a diluted solution in a 5 × 5 mm quartz cuvette.

3. Results and discussion

3.1. Synthesis and characterization of DAHH

The synthesis of the **DAHH** compound was carried out by acid-catalyzed condensation of trans-chalcone and salicylic hydrazide, as shown in Scheme 1, following the previously reported methodology [32]. The structure was confirmed by a combination of spectroscopic (^{1}H, ^{13}C NMR, MS, and FT-IR), thermal (DSC), and single-crystal X-ray diffraction techniques, as detailed in the experimental section and reported in the Supporting Information. The ^{1}H NMR spectrum of the **DAHH** exhibits the expected features with the correct integration ratios. Notably, the proton signal caused by the amide moiety appears as a 1H singlet at 9.2 ppm. In comparison, the proton signal for the double bond system appears at 6.48 ppm as a 1H doublet with *J* = 16.4 Hz, indicating a *trans* configuration (see Figure S1). Also, the mass spectrometry analysis shows a *m/z* peak at 342, consistent with the expected molecular weight (Figure S3). The FT-IR spectrum shows the characteristic bands of the functional groups present in the **DAHH** compound (Figure S4). In the region of 3262 cm^{-1}, a low-intensity band associated with N-H stretching vibration, together with a broad band of O-H at 3055 cm^{-1}, is present. The slight shift towards lower energy is associated with intramolecular and intermolecular hydrogen interactions between the amino group and the phenolic O-H. The vibrations that belong to C=C, C=O, and N=C are observed at 2658, 1638, and 1604 cm^{-1}, respectively. The high intensity band at 1527 cm^{-1} is associated with the –NH–N=C of the hydrazide group. Finally, the DSC analysis shows a small endothermic signal associated with ethanol used to wash the reaction product, with Tonset at 78 °C, followed by a melting endothermic peak at 182 °C, and finally a decomposition endotherm at 202 °C (Figure S5).

3.2. Structural description

Regular block shape crystals suitable for single crystal diffraction were obtained by slow evaporation of a solution of **DAHH** in DCM under room conditions after 24 h. The compound crystallizes in the monoclinic space group $P2_1/c$, with one molecule of the **DAHH** by asymmetric unit (Fig. 1). Crystallographic and refinement parameters are summarized in Table 1. Structurally, the **DAHH** compound consists of a hydrazide group connecting one phenyl ring, one allylic ring, and one phenolic ring. Main bond length parameters are reported in Table 2. The phenyl and phenolic rings exhibit slight distortion around the hydrazide group,

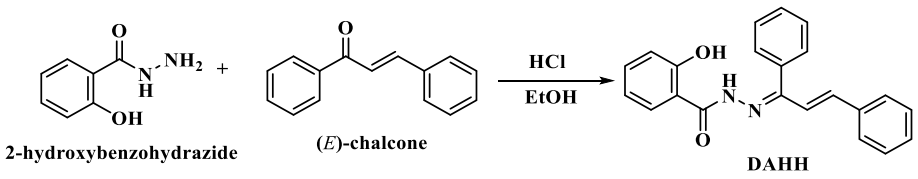

Scheme 1. Synthesis of DAHH.

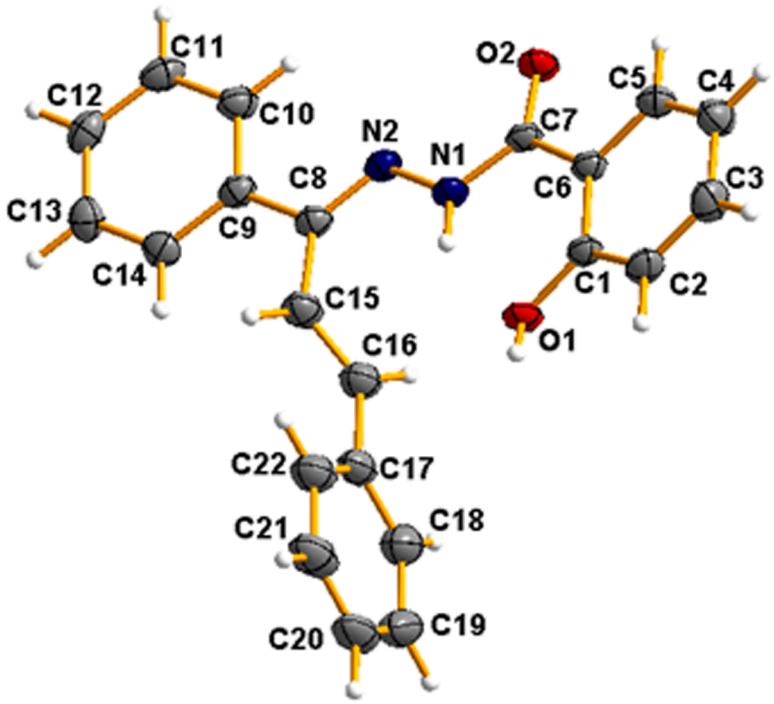

Fig. 1. ORTEP type view of the asymmetric unit of N'-((1Z,2E)-1,3-diphenylallylidene)-2-hydroxybenzohydrazide (**DAHH**) showing thermal ellipsoid at 50 % probability and labeling scheme.

Table 1
Crystallographic and refinement parameters for the **DAHH** compound.

	DAHH
Empirical formula	$C_{22}H_{18}N_2O_2$
Formula weight	342.38
Temperature/K	100.00(11)
Crystal system	Monoclínic
Space group	$P2_1/c$
a/Å	9.2288(1)
b/Å	14.4015(2)
c/Å	12.8462(2)
β (°)	94.290(1)
Volume/ Å^3	1702.586
Z	4
ρ_{calc} mg/mm^3	1.336
μ/mm^{-1}	0.692
F(000)	720
2θ range for data collection/°	9.24 to 159.146
Reflections collected	18,992
Independent reflections	3684 [R(int) = 0.0303]
Data/restraints/parameters	3684/0/243
Goodness-of-fit on F^2	1.055
Completeness (%)	99
Final R indices [$I > 2\sigma(I)$]	R1 = 0.0492, wR2 = 0.1405
Largest diff. Peak/hole/ e.Å^{-3}	−0.3 and 0.38

Table 2
Bond length parameters for **DAHH.**

Atoms	Length (Å)	Atoms	Length (Å)
O1-C1	1.3546(17)	C14-C13	1.391(2)
O2-C7	1.2367(16)	C13-C12	1.385(2)
N1-N2	1.3734(16)	C2-C3	1.378(2)
N1-C7	1.3467(18)	C10-C11	1.387(2)
N2-C8	1.2906(19)	C12-C11	1.385(2)
C7-C6	1.4929(19)	C4-C3	1.392(2)
C9-C8	1.479(2)	C17-C16	1.479(2)
C9-C14	1.394(2)	C17-C18	1.393(3)
C9-C10	1.4057(19)	C17-C22	1.384(3)
C1-C6	1.4104(18)	C15-C16	1.319(2)
C1-C2	1.398(2)	C18-C19	1.391(3)
C6-C5	1.400(2)	C22-C21	1.391(2)
C8-C15	1.4976(19)	C21-C20	1.375(3)
C5-C4	1.378(2)	C19-C20	1.387(3)

with C1-C6-C7-N1 and C10-C9-C8-N2 torsion angles of 7.75(2)° and −3.50(2)°, respectively. Besides, the angle between the plane formed through the phenyl, and the phenolic ring is 17.22° (Figure S7). The allylic group is almost perpendicular to both rings with a C22-C17-C8-N2 torsion angle of 101.26(3)°. The angle between allylic and the hydrazide group is 87.05° (Figure S7). The allylic group presents a non-planar *E* conformation with a C22-C17-C16-C15 torsion angle of −23.00(3)°.

DAHH presents an intramolecular interaction (Table 3) between the amino and the phenol group with a N1-H1A···O1 distance of 2.6407(13) Å. The supramolecular structure is formed mainly by strong O1-H1···O2 interactions with a distance of 2.6168(14) Å, giving rise to infinite chains along [001] direction with a $C_1^1(6)$ graph representation (Fig. 2a).

Table 3
Main hydrogen bond parameters for DAHH.

Atoms	Distance D···A (Å)	Angle (°)	Symmetry
O1-H1···O2	2.6168(14)	160(3)	x,1/2-y,−1/2 + z
N1-H1A···O1	2.6407(15)	139.4(18)	
C2-H2···O2	3.1643(19)	119.00	x,1/2-y,−1/2 + z
C5-H5···O2	2.7533(18)	100.00	

a N2···π interaction with a distance of 3.558(2) Å (Fig. 2b) is also observed. The infinite chains are joined by T-shape C-H···π and C=C···π intermolecular interactions with distances of 3.638(2) Å and 3.485(3) Å, respectively (Fig. 2c), stabilizing the crystal packing (Fig. 2d).

3.3. Hirshfeld surface and fingerprint plot analysis

To visualize and quantify intermolecular interactions, the Hirshfeld surface (HS) and its corresponding fingerprint plot analysis (FPP) were performed [33]. In this case, the dnorm surface is reported, with a color code indicating the proximity of the normalized Van der Waals radii [34]. In this sense, a red region over the oxygen atoms, indicating a strong interaction with distances below the sum of the Van der Waals radii (Fig. 3), is observed. White and blue colors represent interactions equal to or greater than the sum of Van der Waals radii and are associated with the C—H···π, π···π, as well as other weak interactions (Fig. 3). Fig. 3 represent the FPP [35] of DAHH in which it can be observed two peaks at the bottom of the diagram representing the O-H···O strong interactions with an abundance of 10.1%. The most abundant interactions are H···H dispersion interactions with 50.2 %, followed by C···H interactions with 28 % (Fig. 3).

3.4. Lattice energies and energy frameworks

Lattice energies and energy framework analysis of molecular materials allow us to understand the relationship between crystal packing energy and macroscopic properties. In this sense, using the Crystal Explorer software [33], the lattice energy was calculated as the sum of the different interaction energies of the central molecule and its neighbors within a 3.8 Å radius [36]. Electron density values were calculated using a B3LYP/6–31G(d,p) level of theory with E_{ele}= 1.057, E_{pol}= 0.740, E_{disp}= 0.871, and E_{rep}= 0.618 scale factors. Lattice energy values are presented in Fig. 4, where N represents the number of molecules with the exact symmetry and energy, R represents the distance between the molecular centroids in Å, and the energies of the interactions are in kJ/mol[37]. The highest E_{total} interaction values are observed between the central molecule (black) and both navy blue and light green molecules, with values of −67.8 and −87.8 kJ/mol, respectively (Fig. 4). In both cases, the significant contributions correspond to dispersion and electrostatic energies, which agree with the interactions observed in the supramolecular analysis, since the interactions with the highest abundance were H···H, C···H, and O-H···O.

Energy frameworks depict intermolecular energies in crystal packing as a cylinder whose width represents their magnitude [38]. These frameworks also show clearly the formation of ladders by O-H···O associated with coulombic energy and H···H and C···H interactions, associated with dispersion energy, and the sum of all the interactions as total energy representation (Fig. 5).

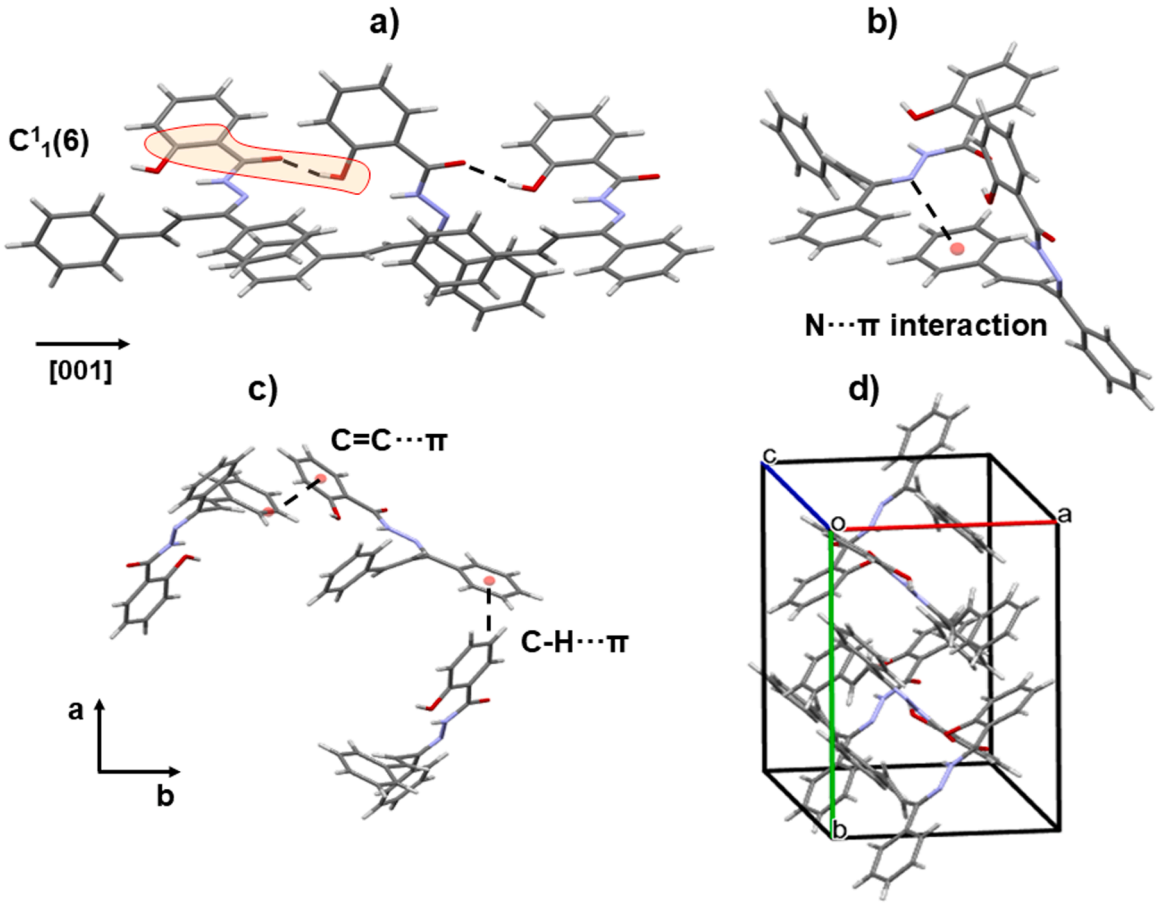

Fig. 2. Representation of a) infinite chains along [001] direction formed by O-H···O strong hydrogen bonds, b) N2···π, c) C-H···π and C=C···π intermolecular interactions and d) **DAHH** crystal packing.

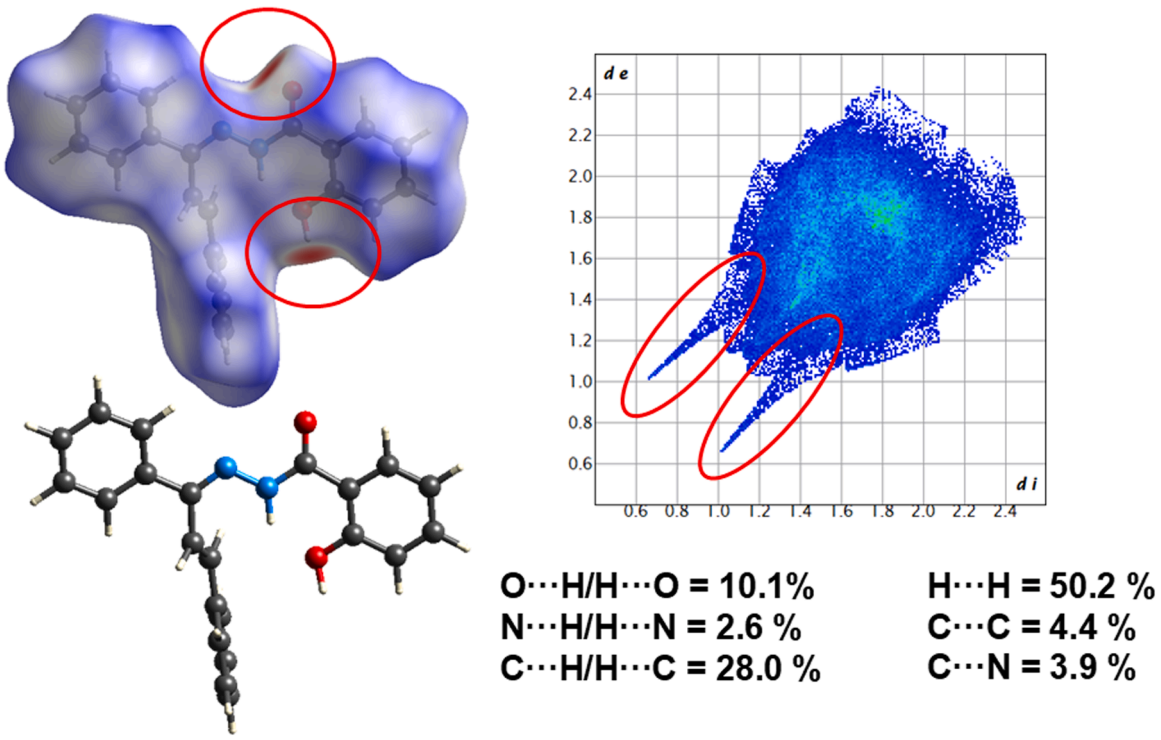

Fig. 3. Hirshfeld surface analysis (HS) represented by d_{norm} surface and fingerprint plot analysis (FPP) with the quantification of the interactions presents in the **DAHH** molecular crystal. Red circles indicate the N···H/ H···N interactions in d_{norm} surface and FPP.

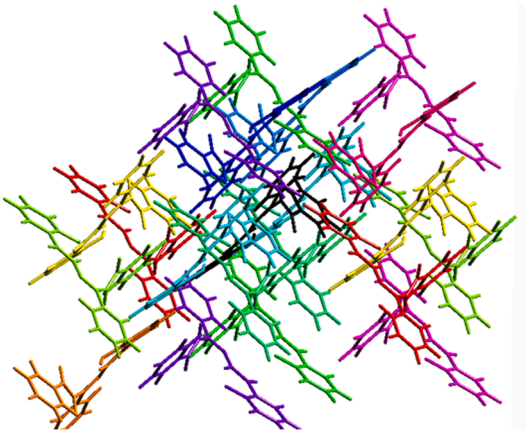

	N	Symop	R	E_ele	E_pol	E_dis	E_rep	E_tot
	2	x, -y+1/2, z+1/2	11.06	-4.6	-1.1	-16.9	14.8	-11.2
	1	-x, -y, -z	14.24	-3.0	-0.4	-4.4	0.0	-7.3
	2	x, y, z	9.23	1.7	-0.8	-10.3	3.2	-5.8
	2	x, -y+1/2, z+1/2	11.84	-3.4	-0.8	-12.5	9.8	-9.1
	2	-x, y+1/2, -z+1/2	8.09	-8.4	-1.8	-36.4	25.4	-26.2
	2	x, -y+1/2, z+1/2	6.79	-79.5	-24.8	-56.4	103.1	-87.8
	2	x, y, z	12.85	-3.4	-0.5	-6.2	0.0	-9.4
	1	-x, -y, -z	11.21	2.1	-0.7	-6.3	2.7	-2.1
	1	-x, -y, -z	5.84	-16.4	-6.7	-87.4	49.4	-67.8
	2	-x, y+1/2, -z+1/2	11.78	-1.1	-3.4	-9.3	5.5	-8.3
	2	-x, y+1/2, -z+1/2	11.79	-0.3	-0.2	-3.0	0.5	-2.7
	1	-x, -y, -z	9.94	-2.8	-0.5	-27.6	12.3	-19.7

Fig. 4. Crystal packing around one central molecule (black) of **DAHH**. The color representation of each molecule surrounding is associated with the values of energy (kJ/mol) in the table.

3.5. Photoluminescence Analysis

The **DAHH** molecule is composed of different functional groups, distinguished by high conjugation, aromatic rings, and electron-donating atoms. The presence of aromatic rings and double bonds in the structure confers high structural stability and unique electronic properties. The electronic processes involved in energy absorption and emission are well known and include the promotion of electrons from the S0 ground state to excited electronic states, followed by relaxation processes such as fluorescence, intersystem crossing, and/or phosphorescence. In this case, it is possible to observe in the absorption spectrum (341 nm) one broad band which contains transitions associated with $\pi \rightarrow \pi^*$ excitation of the aromatic and double bond systems, and $n \rightarrow \pi^*$ electronic transitions related to the presence of groups with non-bonding electrons such as hydrazide and -OH groups (Fig. 6).

It is important to note that although the **DAHH** compound lacks a planar structure, the presence of three aromatic rings with electron-donating functional groups results in a single emission band at 511 nm, as expected for arylhydrazine derivatives [39]. Photoluminescence can be characterized using the Commission Internationale de l'Eclairage (CIE) x,y coordinates to compare light-emission performance and to identify potential luminescence applications [40]. The color of the emission of **DAHH** can be characterized using the CIE x,y chromaticities system 2D diagram (Fig. 6) and shows a greenish-turquoise color emission with CIE-coordinates of $x = 0.30$, $y = 0.49$. Color purity is a measure of color's saturation from the CIE 1931 chromaticity diagram

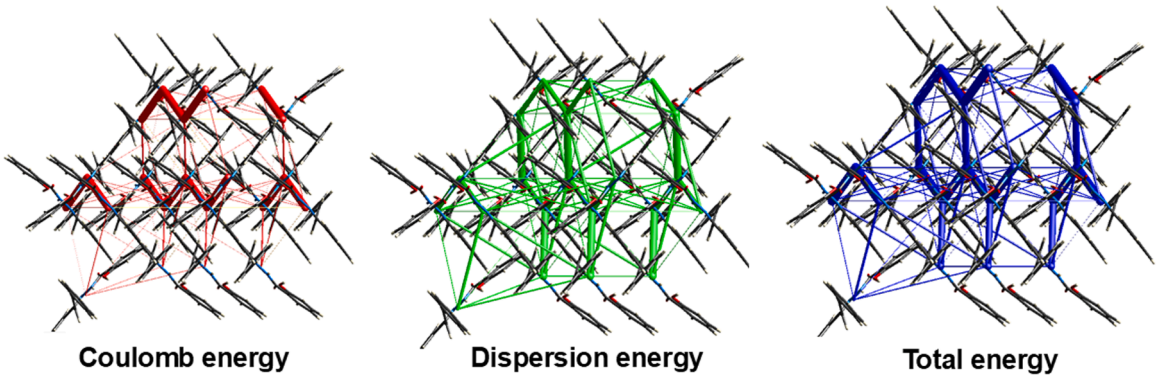

Fig. 5. Energy frameworks for the most important interactions that contribute to total energy in the crystal packing for the **DAHH** compound.

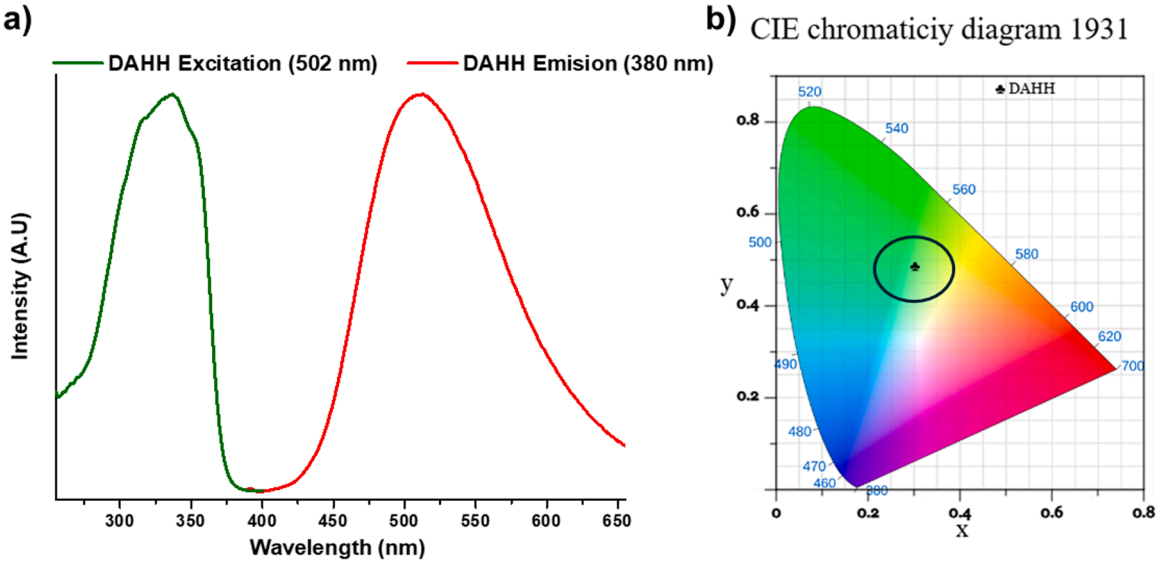

Fig. 6. a) Excitation (green) and emission (red) spectrum, and b) CIE x,y chromaticities system 2D diagram for **DAHH** compound. Emission was recorded using an excitation wavelength set to 350 nm, an integration time of 1s per data point and a, scanning speed of 1 nm/s, slit width of 3.0 nm bandpass and a grating with 1200 lines/mm. The excitation spectrum was recorded for detection at 502 nm, 1nm/s; 2,0 nm bandpass and proved to be independent of the detection wavelength. Excitation and absorption spectra are in accordance, cf. Supporting Information S6.

and was determined to be 30.52 %. This value indicates the color purity as a percentage based on the ratio of two-line segments on the diagram: the distance from the white point to the sample's color, and the distance from the white point to the color's dominant wavelength, with the formula:

$$color\ purity = \frac{\sqrt{(x-x_s)^2+(y-y_s)^2}}{\sqrt{(x_d-x_s)^2+(y_d-y_s)^2}} \cdot 100$$

The corresponding CIE coordinates, i.e. x_s, y_s for standard white, x_d, y_d for the dominant wavelength and x,y, for the sample. The spectral properties of **DAHH** are comparable to those of Alq_3, one of the most widely used green-emitting molecules in OLEDs [41].. The tris (8-hydroxyquinoline)aluminum typically emits in the green region, with peaks around 520–530 nm and CIE coordinates $x = 0.27$, $y = 0.50$. Further emitters used in applications based on Schiff base complexes, such as Zn complexes with derivatives of salicylaldehyde and o-vanillin as ligands were also reported [42]. The applicability of an emitter in an OLED device depends on many factors such as emission efficiency, color purity, stability of the compound during OLED device fabrication as well as operation. Thus, the presented data are not sufficient to prove the applicability of **DAHH** as an emitter in an OLED device, but this new compound demonstrates its potential in this application.

4. Conclusion

We report the synthesis of a new benzohydrazide derivative, *N*'-((1*Z*,2*E*)-1,3-diphenylallylidene)-2-hydroxybenzohydrazide (**DAHH**), from *trans*-chalcone and salicylic hydrazide. The ^{1}H NMR spectrum shows the characteristic signal for the amide proton, indicating the formation of the expected product. The crystal structure presents a distortion between the planes through the rings. The molecular conformation is stabilized by an N-H···O intramolecular interaction between the amino and the phenol group. N-H···O and O-H···O interactions, as well as weak T-shaped C-H···π and C=C···π interactions, consolidate the crystal packing. These interactions were quantified using Hirshfeld surface and fingerprint plot analysis, finding that the most abundant interactions are H···H dispersion interactions at 50.2 %, followed by C···H at 28 % and O···H at 10.1 %. The crystal packing was also analyzed in terms of lattice energies, finding that the significant contribution arises from the dispersion and electrostatic terms, in agreement with the supramolecular analysis. Finally, the study of the electronic and optical properties shows one emission band at 512 nm, with the CIE x,y chromaticity diagram showing greenish-turquoise color emission at $x = 0.3$, $y = 0.486$. This new molecule is a potential material for applications such as organic light-emitting diodes (OLEDs) and optical sensors.

CRediT authorship contribution statement

David Oliveros Garavito: Methodology, Investigation. **Andrea Pastrana-Dávila:** Investigation, Formal analysis. **Javier Ellena:** Supervision, Software, Methodology, Funding acquisition, Data curation. **Pedro H.O. Santiago:** Validation, Formal analysis, Data curation. **Oscar Rojas:** Visualization, Validation, Methodology, Investigation, Funding acquisition, Formal analysis, Data curation. **Dominik Pentlehner:** Validation, Supervision, Software, Resources, Project administration, Methodology, Investigation, Funding acquisition, Formal analysis, Data curation. **Luis A. Illicachi:** Writing – review & editing, Writing – original draft, Validation, Project administration, Methodology, Investigation, Funding acquisition, Formal analysis, Conceptualization. **Richard D'Vries:** Writing – review & editing, Writing – original draft, Visualization, Validation, Investigation, Funding acquisition, Formal analysis, Data curation, Conceptualization.

Declaration of competing interest

The authors declare that they have no known competing financial interests or personal relationships that could have appeared to influence the work reported in this paper.

Acknowledgments

D.O.G. and L.I. acknowledge Universidad Santiago de Cali for the DGI project 939-621124-749 (Fortalecimiento de Grupos 2024 -QUIBIO). R.D. acknowledges Universidad del Cauca for the project ID-6161. R.D., A.P-D., O.R., and D.P. are very grateful to BayLat start-up financing 2024 for new research projects between Colombia and Germany. J.E. is thankful to the Brazilian agencies FAPESP (Process No. 2017/15850-0) and CNPq (Process No. 312505/2021-3).

Supplementary materials

Supplementary material associated with this article can be found, in the online version, at doi:10.1016/j.molstruc.2025.145191.

Data availability

Data will be made available on request.

References

[1] M. Alizadeh, A. Kariminik, A. Akbari, Synthesis and characterization of chemical compounds derived from benzohydrazide and evaluation of their antibacterial activities, Avicenna J. Clin. Microbiol. Infect. 8 (1) (2021) 5–10, https://doi.org/10.34172/ajcmi.2021.02.

[2] M.H. Mahnashi, P. Koganole, S.R. PK, S.S. Ashgar, I.A. Shaikh, S.D. Joshi, A. S. Alqahtani, Synthesis, molecular docking study, and biological evaluation of new 4-(2,5-Dimethyl-1H-pyrrol-1-yl)-N'-(2-(substituted)acetyl)benzohydrazides as dual enoyl ACP reductase and DHFR enzyme inhibitors, Antibiotics 12 (4) (2023) 763, https://doi.org/10.3390/antibiotics12040763.

[3] M. Vilková, M. Hudáčová, N. Palušeková, R. Jendželovský, M. Almáši, T. Béres, P. Fedoročko, M. Kožurková, Acridine based N-acylhydrazone derivatives as potential anticancer agents: synthesis, characterization and ctDNA/HSA spectroscopic binding properties, Molecules 27 (9) (2022) 2883, https://doi.org/10.3390/molecules27092883.

[4] Y. Biliz, B. Hasdemir, H. Başpınar Küçük, M. Zaim, A.M. Şentürk, A. Müdüroğlu Kırmızıbekmez, İ. Kara, Novel N-Acyl, Hydrazone compounds as promising anticancer agents: synthesis and molecular docking studies, ACS Omega 8 (22) (2023) 20073–20084, https://doi.org/10.1021/acsomega.3c02361.

[5] E. Świętczak, M. Rachwalski, A.M. Pieczonka, Eco-friendly methods for the synthesis of N-acyl pyrazole derivatives with luminescent properties, RSC Adv. 15 (16) (2025) 12698–12703, https://doi.org/10.1039/D4RA08527B.

[6] T. Liu, Z. Xie, T. Zhang, Y. Wen, S. Xue, W. Shi, Facile synthesis of acyl-hydrazone composites based on hydrazide-modified formylated polystyrene for effective removal of heavy metal ions and sulfides from water, ACS Appl. Mater. Interfaces 17 (1) (2025) 1049–1063, https://doi.org/10.1021/acsami.4c16530.

[7] G.-F. Liu, Z.-W. Li, Z.-J. Huang, Z. Zhou, Y.-X. Li, A. Huang, Z. Cai, G. Ouyang, B.-H. Ye, Y.-B. Zhang, Rapid crystallization and versatile metalation of acetylhydrazone-linked covalent organic frameworks for heterogenous catalysis, J. Am. Chem. Soc. 147 (2) (2025) 1840–1850, https://doi.org/10.1021/jacs.4c13982.

[8] M.S. Mahfouz, A.A.M. Ali, M. Shebl, O.M.I. Adly, R. Fouad, Copper(ii) chelates of a coumarin-based acyl hydrazone ligand: structural characterization and computational evaluations for prospective applications in antimicrobial, antiviral, antioxidant, and anticancer therapies, RSC Adv. 15 (28) (2025) 22972–22988, https://doi.org/10.1039/D5RA03317A.

[9] C.C. Carmona-Vargas, S.L. Aristizábal, M.I. Belalcázar, R.F. D'Vries, M.N. Chaur, Determination of the binding constants of propeller-like metal complexes of picolinaldehyde-2-pyridylhydrazone, Inorganica Chim. Acta 487 (2019) 275–280, https://doi.org/10.1016/j.ica.2018.12.026.

[10] X. Su, I. Aprahamian, Hydrazone-based switches, metallo-assemblies and sensors, Chem. Soc. Rev. 43 (6) (2014) 1963–1981, https://doi.org/10.1039/C3CS60385G.

[11] S. Fernández-Palacios, E. Matamoros, I.Morato Rojas, J.T. López Navarrete, M. C. Ruiz Delgado, Y. Vida, E. Perez-Inestrosa, New insights into acylhydrazones E/Z isomerization: an experimental and theoretical approach, Int. J. Mol. Sci. 24 (19) (2023) 14739, https://doi.org/10.3390/ijms241914739.

[12] K. Pradeep, N. Balasubramanian, R. Kalavathy, M. Vasudevan, M. Rakesh Kumar, M. Abu Bakar Abdul, Synthesis, antimicrobial, anticancer evaluation and QSAR studies of 3/4-bromo benzohydrazide derivatives, Curr. Top. Med. Chem. 15 (11) (2015) 1050–1064, https://doi.org/10.2174/1568026615111504081112 52.

[13] T.A. Yousef, L.H.K. Al-Jibori, A.S. Fiahan, A.O. Elzupir, M.M. Abou-Krisha, A.S. M. Al-Janabi, Benzohydrazide derivative metal complex's antimicrobial and inhibitory effects on liver cancer cell lines and quinone oxidoreductase 2: experimental, molecular docking, and DFT investigations, J. Mol. Struc. 1308 (2024) 138073, https://doi.org/10.1016/j.molstruc.2024.138073.

[14] Y. Sawada, T. Yanai, H. Nakagawa, Y. Tsukamoto, S. Yokoi, M. Yanagi, T. Toya, H. Sugizaki, Y. Kato, H. Shirakura, T. Watanabe, Y. Yajima, S. Kodama, A. Masui, Synthesis and insecticidal activity of benzoheterocyclic analogues of N′-benzoyl-N-(tert-butyl)benzohydrazide: part 2. Introduction of substituents on the benzene rings of the benzoheterocycle moiety, Pest Manag. Sci. 59 (1) (2003) 36–48, https://doi.org/10.1002/ps.605.

[15] S. Liu, H. Li, S. Li, M. Sun, X. Bao, Discovery of new benzohydrazide derivatives containing 4-aminoquinazoline as effective agricultural fungicides, the related mechanistic study, and safety assessment, J. Agric. Food Chem. 73 (5) (2025) 2830–2841, https://doi.org/10.1021/acs.jafc.4c09461.

[16] İ. Sıdır, Y.G. Sıdır, H. Berber, F. Demiray, Electronic structure and optical properties of Schiff base hydrazone derivatives by solution technique for optoelectronic devices: synthesis, experiment and quantum chemical investigation, J. Mol. Struc. 1176 (2019) 31–46, https://doi.org/10.1016/j.molstruc.2018.08.067.

[17] T.K. Kavya Bodhi, R. Tamizhselvi, S. Mohandoss, A. Arumugam Napoleon, Novel benzohydrazide-based Schiff base for highly selective and sensitive colorimetric detection of Hg2+ ions; DFT analysis and test strips applications, Inorg. Chem. Commun. 159 (2024) 111649, https://doi.org/10.1016/j.inoche.2023.111649.

[18] R.S. Moraes, R.E. Aderne, M. Cremona, N.A. Rey, Luminescent properties of a dihydrazone derived from the antituberculosis agent isoniazid: potentiality as an emitting layer constituent for OLED fabrication, Opt. Mater. 52 (2016) 186–191, https://doi.org/10.1016/j.optmat.2015.12.039.

[19] A.I. Kornikov, R.E. Mustakimov, A.S. Goloveshkin, L.O. Tcelykh, A.A. Vashchenko, A.V. Medvedko, L.S. Lepnev, V.V. Utochnikova, Novel ytterbium Schiff base complex: toward efficient solution-processed NIR-emitting OLED, Org. Electron. 105 (2022) 106492, https://doi.org/10.1016/j.orgel.2022.106492.

[20] P. Wang, J. Liu, X. Lv, Y. Liu, Y. Zhao, W. Guo, A naphthalimide-based glyoxal hydrazone for selective fluorescence turn-on sensing of cys and hcy, Org. Lett. 14 (2) (2012) 520–523, https://doi.org/10.1021/ol203123t.

[21] S. Suganya, S. Velmathi, P. Venkatesan, S.-P. Wu, M.S. Boobalan, A highly fluorescent zinc complex of a dipodal N-acyl hydrazone as a selective sensor for H2PO4− ions and application in living cells, Inorg. Chem. Front. 2 (7) (2015) 649–656, https://doi.org/10.1039/C5QI00036J.

[22] D.C. Santos, P.J.S. Maia, M.A. de Abreu Lopes Jr, J.S.B. Forero, A.L.F. de Souza, A simple isoniazid-based N-acylhydrazone derivative as potential fluorogenic probe for Zn2+ ions, J. Fluoresc. 31 (1) (2021) 175–184, https://doi.org/10.1007/s10895-020-02651-7.

[23] H.J. Cho, T. Kim, H. Kim, C. Song, Solid-State emissive metallo-supramolecular assemblies of quinoline-based acyl hydrazone, Sensors 20 (3) (2020) 600, https://doi.org/10.3390/s20030600.

[24] CrysAlisPro, CrysAlisPro, in: A.T. Ltd (Ed.) Agilent Technologies Ltd, Yarnton, Oxfordshire, England, 2014.

[25] G. Sheldrick, SHELXT - integrated space-group and crystal-structure determination, Acta Cryst. A 71 (1) (2015) 3–8, https://doi.org/10.1107/S2053273314026370.

[26] G. Sheldrick, Crystal structure refinement with SHELXL, Acta Cryst. C 71 (1) (2015) 3–8, https://doi.org/10.1107/S2053229614024218.

[27] O.V. Dolomanov, L.J. Bourhis, R.J. Gildea, J.A.K. Howard, H. Puschmann, OLEX2: a complete structure solution, refinement and analysis program, J. Appl. Crystallogr. 42 (2) (2009) 339–341, https://doi.org/10.1107/S0021889808042726.

[28] R.H.-I. Peter Muller, Anthony Spek, Thomas Schneider, Michael Sawaya, Crystal Structure Refinement: A Crystallographer's Guide to SHELXL, Oxford University Press Inc., New York, 2006.

[29] G. Sheldrick, A short history of SHELX, Acta Cryst. A 64 (1) (2008) 112–122, https://doi.org/10.1107/S0108767307043930.

[30] K. Brandenburg, H. Putz, , DIAMOND- crystal and molecular structure visualization, in: C. Impact (Ed.) DIAMOND, Crystal Impact, Kreuzherrenstr. 102, 53227 Bonn, Germany, 2006.

[31] C.F. Macrae, I.J. Bruno, J.A. Chisholm, P.R. Edgington, P. McCabe, E. Pidcock, L. Rodriguez-Monge, R. Taylor, J. Van De Streek, P.A. Wood, Mercury CSD 2.0–new features for the visualization and investigation of crystal structures, J. Appl. Crystallogr. 41 (2) (2008) 466–470, https://doi.org/10.1107/S0021889807067908.

[32] A. Aljuhani, M.S. Nafie, N.R. Albujuq, M. Alsehli, S.K. Bardaweel, K.M. Darwish, S. Y. Alraqa, M.R. Aouad, N. Rezki, Discovery of new benzothiazole-1,2,3-triazole hybrid-based hydrazone/thiosemicarbazone derivatives as potent EGFR inhibitors with cytotoxicity against cancer, RSC Adv. 15 (5) (2025) 3570–3591, https://doi.org/10.1039/D4RA07540D.

[33] P.R. Spackman, M.J. Turner, J.J. McKinnon, S.K. Wolff, D.J. Grimwood, D. Jayatilaka, M.A. Spackman, CrystalExplorer: a program for Hirshfeld surface analysis, visualization and quantitative analysis of molecular crystals, J. Appl. Crystallogr. 54 (3) (2021) 1006–1011, https://doi.org/10.1107/S1600576721002910.

[34] J.J. McKinnon, M.A. Spackman, A.S. Mitchell, Novel tools for visualizing and exploring intermol-ecular interactions in molecular crystals, Acta Cryst. B 60 (6) (2004) 627–668.

[35] M.A. Spackman, J.J. McKinnon, Fingerprinting intermolecular interactions in molecular crystals, CrystEngComm 4 (66) (2002) 378–392, https://doi.org/10.1107/S0108768104020300.

[36] C.F. Mackenzie, P.R. Spackman, D. Jayatilaka, M.A. Spackman, CrystalExplorer model energies and energy frameworks: extension to metal coordination compounds, organic salts, solvates and open-shell systems, IUCrJ 4 (5) (2017) 575–587, https://doi.org/10.1039/B203191B.

[37] M.J. Turner, S. Grabowsky, D. Jayatilaka, M.A. Spackman, Accurate and efficient model energies for exploring intermolecular interactions in molecular crystals, J. Phys. Chem. Lett. 5 (24) (2014) 4249–4255.

[38] M.J. Turner, S.P. Thomas, M.W. Shi, D. Jayatilaka, M.A. Spackman, Energy frameworks: insights into interaction anisotropy and the mechanical properties of molecular crystals, Chem. Commun. 51 (18) (2015) 3735–3738, https://doi.org/10.1021/jz502271c.

[39] P. Sobczak, T. Sierański, M. Świątkowski, A. Trzęsowska-Kruszyńska, J. Kolińska, Unraveling the structure–property relationships in fluorescent phenylhydrazones: the role of substituents and molecular interactions, RSC Adv. 15 (2025) 1514–1526, https://doi.org/10.1039/D4RA07856J.

[40] E.H.H. Hasabeldaim, H.C. Swart, R.E. Kroon, Luminescence and stability of Tb doped CaF2 nanoparticles, RSC Adv. 13 (8) (2023) 5353–5366, https://doi.org/10.1039/D2RA07897J.

[41] S. Kagatikar, D. Sunil, Schiff bases and their complexes in organic light emitting diode application, J. Electron. Mater. 50 (12) (2021) 6708–6723, https://doi.org/10.1007/s11664-021-09197-9.

[42] L. Lepnev, A. Vaschenko, A. Vitukhnovsky, S. Eliseeva, O. Kotova, N. Kuzmina, OLEDs based on some mixed-ligand terbium carboxylates and zinc complexes with tetradentate Schiff bases: mechanisms of electroluminescence degradation, Synth. Met. 159 (7) (2009) 625–631, https://doi.org/10.1016/j.synthmet.2008.12.006.